Original Article

# *ATP5A1* as a potential prognostic biomarker in clear-cell renal cell carcinoma

**Wei Zhou[1,2]^, Qianli Tang[3], Jun Wu[2], Minyu Huang[2], Qun Huang[2], Tianzi Qin[2], Ning Tang[4], Shasha Gai[4]**

[1]Graduate School of the First Clinical Medical College of Jinan University, Guangzhou, China; [2]Department of Urology, the Affiliated Hospital of Youjiang Medical University for Nationalities, Baise, China; [3]Key Laboratory of Tumor Molecular Pathology of Baise, Affiliated Hospital of Youjiang Medical University for Nationalities, Baise, China; [4]Graduate School of Youjiang Medical University for Nationalities, Baise, China

*Contributions:* (I) Conception and design: W Zhou, Q Tang; (II) Administrative support: J Wu, Q Huang; (III) Provision of study materials or patients: M Huang; (IV) Collection and assembly of data: W Zhou, T Qin; (V) Data analysis and interpretation: W Zhou, N Tang, S Gai; (VI) Manuscript writing: All authors; (VII) Final approval of manuscript: All authors.

*Correspondence to:* Qianli Tang, MD. Key Laboratory of Tumor Molecular Pathology of Baise, Affiliated Hospital of Youjiang Medical University for Nationalities, 18 Zhongshan 2nd Rd, Baise 533000, China. Email: htmgx@ymun.edu.cn.

**Background:** Clear cell renal cell carcinoma (ccRCC), a malignant neoplasm originating in the renal tubules, is characterized by extended treatment durations and suboptimal therapeutic outcomes in clinical settings. Adenosine triphosphate (ATP) synthase F1 subunit α (*ATP5A1*), a subunit of mitochondrial ATP synthase, is integral to the energy metabolism of specific tumors. While prior research has established a link between *ATP5A1* expression and malignancies, its precise function and clinical significance in ccRCC are yet to be elucidated. The study aims to investigate the role of ATP5A1 in ccRCC and to explore the underlying molecular mechanisms.

**Methods:** The RNA sequencing data from ccRCC and corresponding adjacent tissues were analyzed through The Cancer Genome Atlas to evaluate their diagnostic and prognostic implications. *ATP5A1* expression in ccRCC was validated using the Human Protein Atlas database. The role of *ATP5A1* in ccRCC was further characterized through a series of assays, including wound healing, transwell invasion, cell counting kit-8 proliferation, and flow cytometry.

**Results:** *ATP5A1* expression levels were elevated across 17 tumor types while being notably downregulated in 15 others, including ccRCC, esophageal carcinoma, and colon adenocarcinoma. Compared to 293 cells and adjacent normal kidney tissues, renal cancer cells and tissues exhibited a significant reduction in *ATP5A1* expression. An inverse relationship was observed between *ATP5A1* expression and both the clinical stage and histological grade of ccRCC, yet it is positively associated with improved prognosis. Silencing *ATP5A1* expression enhanced the malignant biological properties of ccRCC, while its upregulation inhibited these effects. Furthermore, *ATP5A1* knockdown activated the Wnt/β-catenin signaling pathway, whereas its overexpression resulted in pathway suppression.

**Conclusions:** Collectively, this study indicates that *ATP5A1* may serve as a potential biomarker for the diagnosis, prognosis, and therapeutic targeting of ccRCC.

**Keywords:** Adenosine triphosphate synthase F1 subunit α (*ATP5A1*); clear cell renal cell carcinoma (ccRCC); bioinformatic analysis; biomarker

Submitted Aug 10, 2024. Accepted for publication Dec 17, 2024. Published online Feb 26, 2025.
doi: 10.21037/tcr-24-1397
**View this article at:** https://dx.doi.org/10.21037/tcr-24-1397

^ ORCID: 0009-0006-6395-1219.

## Introduction

Renal cancer represents approximately 5% of malignant tumors in adult males and 3% in adult females, with clear cell renal cell carcinoma (ccRCC) being the predominant subtype. The insidious nature of renal cancer leads to over 50% of cases being detected incidentally (1). While surgical intervention offers curative potential in early-stage ccRCC, the mortality rate escalates significantly upon metastasis. The absence of von Hippel Lindau (VHL) alleles is a hallmark of ccRCC, leading to the overexpression of downstream genes, which are critical therapeutic targets for ccRCC management (2,3). Conventional chemotherapy proves largely ineffective against ccRCC, whereas targeted therapy has emerged as the preferred non-surgical treatment due to its specificity, low toxicity, and potential to enhance patient survival (4). Consequently, the integration of bioinformatics with experimental validation is anticipated to facilitate the identification of novel biomarkers and therapeutic targets for ccRCC.

Adenosine triphosphate (ATP) synthase is a fundamental enzyme responsible for energy production across a wide range of organisms. Based on its functional characteristics, ATP synthase is categorized into several types: F, V, A, P, and E. The F-type ATP synthase, also referred to as F1F0 ATP, consists of two structural domains, F [1] and F [0]. This enzyme is predominantly located in the inner mitochondrial membrane and plays a key role in ATP synthesis (5). The ATP synthase F1 subunit α (*ATP5A1*) gene encodes the α subunit of the ATP synthase complex, which promotes the conversion of adenosine diphosphate (ADP) and inorganic phosphate (Pi) into ATP, thereby playing an essential role in intracellular energy production. However, *ATP5A1* expression levels differ among various tumor types, leading to distinct impacts on malignant cells. Elevated *ATP5A1* expression in hepatocellular carcinoma correlates with the activation of oncogenic pathways (6), while targeted microRNA (miRNA)-induced downregulation of *ATP5A1* enhances glioblastoma tumor aggressiveness (7). Additionally, the role of ATP5A1 in colon cancer is to affect mitochondrial function through its interaction with SIRT3 and its deacetylation state, thereby influencing the growth and survival of colon cancer cells (8). Conversely, reduced *ATP5A1* expression has been observed in renal tumors (9), suggesting a potential role in ccRCC progression through modifications in tumor-associated phosphorylation (10). Wnt/β-catenin signaling plays a critical role in the initiation and progression of kidney carcinoma, with VHL identified as a target of β-catenin within this pathway, emphasizing its significance in renal cancer development (11). While extensive research has established a strong correlation between *ATP5A1* and various tumors, its specific involvement in renal cancer remains underexplored. This study utilized bioinformatics analysis alongside cellular assays to investigate the Pathophysiological function of *ATP5A1* in ccRCC, aiming to uncover potential therapeutic targets for this malignancy. We present this article in accordance with the TRIPOD reporting checklist (available at https://tcr.amegroups.com/article/view/10.21037/tcr-24-1397/rc).

### Highlight box

**Key findings**

- Adenosine triphosphate synthase F1 subunit α (*ATP5A1*) demonstrates potential as a prognostic biomarker in clear cell renal cell carcinoma (ccRCC).

**What is known and what is new?**

- Previous studies suggested that *ATP5A1* expression was reduced in ccRCC, but the specific mechanisms were not elucidated.
- Our research reveals that *ATP5A1* potentially impacts the migration, proliferation, invasion, and apoptosis of ccRCC through the suppression of the Wnt/β-catenin signaling pathway.

**What is the implication, and what should change now?**

- Further investigation is necessary to elucidate the impact of *ATP5A1* on the Wnt/β-catenin signaling pathway.

## Methods

### *Public data access*

The Cancer Genome Atlas (TCGA) (https://www.cancer.gov/ccg/research/genome-sequencing/tcga) provided the foundational bioinformatics data for this study. Comparative analysis of *ATP5A1* expression between ccRCC and normal kidney tissues was conducted using data from the Human Protein Atlas (HPA) (https://www.proteinatlas.org/). Additionally, co-expression genes of *ATP5A1* in ccRCC were identified through the Cbioportal database (http://www.cbioportal.org/). The study was conducted in accordance with the Declaration of Helsinki (as revised in 2013).

### *Cell lines*

Human renal cancer cell lines 786-O, CAKI-1, 769-P, and human embryonic kidney cell lines 293 cells were

**Table 1** Primers for RT-PCR analysis

| Gene | Forward primer, 5'-3' | Reverse primer, 5'-3' |
|---|---|---|
| *ATP5A1* | TCGTGTAGTTGATGCCCTTG | TCCCGCACTGAAATTCG |
| *GAPDH* | CAGGAGGCATTGCTGATGAT | CAGGAGGCATTGCTGATGAT |

RT-PCR, reverse transcription-polymerase chain reaction.

purchased from Wuhan Pricella Biotechnology Co., Ltd. (Wuhan, China). The authentication of the experimental cells was performed using human short-tandem repeat (STR) analysis, and this was followed by a thorough screening for mycoplasma contamination in all cell lines. The cells were maintained in Gibco® RPMI 1640 and Procell™ McCoy's 5A media, supplemented with 10% fetal calf serum and 1% penicillin-streptomycin, and incubated at 37 ℃ with 5% $CO_2$.

### *Reverse transcription-quantitative polymerase chain reaction (RT-qPCR) analysis*

Total RNA extraction from the cell lines was performed using TRIzol® reagent, followed by RT utilizing a cDNA assay kit (Tolobio, Anhui, China). RT-qPCR was subsequently conducted with an SYBR assay kit under the following thermocycling conditions: initial denaturation at 95 ℃ for 30 s, followed by 40 cycles of denaturation at 95 ℃ for 10 s, and combined annealing and extension at 60 ℃ for 30 s. Data quantification was achieved via the $2^{-\Delta\Delta Cq}$ method (12). The primer sequences utilized in these experiments were listed in *Table 1*.

### *Western blot (WB) assay*

Total protein extraction from the cell lines was conducted using radio immunoprecipitation assay (RIPA) lysis buffer, with protein concentration quantified via a bicinchoninic acid (BCA) kit (EpiZyme, Shanghai, China) according to the manufacturer's protocol. Proteins were denatured by boiling at 100 ℃ for 10 minutes. A consistent 30 μg of protein was loaded per gel lane for separation through sodium dodecyl sulfate polyacrylamide gel electrophoresis (SDS-PAGE) (EpiZyme), followed by transfer onto a 0.45 μm polyvinylidene fluoride (PVDF) membrane. The membrane was blocked with a protein-free solution (EpiZyme) at room temperature for 30–60 minutes, then incubated with primary antibodies against ATP5A1 (Abcam, Cambridge, UK; ab176569, 1:10,000), phosphorylated (p)-GSK3β (Zenbioscience, Chengdu, China; 310010, 1:1,000), β-catenin (Zenbioscience, R23616, 1:1,000), c-Myc (Zenbioscience, R22809, 1:1,000), and glyceraldehyde-3-phosphate dehydrogenase (GAPDH) (Zenbioscience, R24404, 1:1,000) at 4 ℃ for 12–18 hours. The membrane was then incubated with the secondary antibody (Proteintech, Wuhan, China; SA00001-2, 1:2,000) for 1 hour at room temperature. Visualization was achieved using an enhanced chemiluminescence (ECL) luminescent kit (EpiZyme, SQ202).

### *Immunofluorescence assay*

Four types of cells were evenly seeded into 12-well plates, with 80,000 to 100,000 cells per well. After the cells adhered firmly to the well walls, the medium was removed, and cells were fixed with 4% paraformaldehyde for 10 minutes, followed by phosphate buffered saline (PBS) washing. Cells were then permeabilized with 5% Triton X-100 for 20 minutes and washed with PBS for 15 seconds. Following this, the cells were blocked with 2% bovine serum albumin (BSA) for 30 minutes, and primary antibody against ATP5A1 was applied. Incubation was carried out at 4 ℃ for 12–18 hours. The cells were washed three times with PBS (15 seconds per wash) before the fluorescent secondary antibody was added, followed by a 1-hour incubation at room temperature. After an additional wash, nuclei were stained with DAPI for 5 minutes, and the results of the immunofluorescence assay were observed using a fluorescence microscope. Fluorescence detection results were analyzed using NIS-Elements Viewer software. The expression level of ATP5A1 was quantified by comparing the mean fluorescence intensities among the different cell groups.

### *Cell transduction studies*

Both ATP5A1 siRNA (Si-NC or Si-ATP5A1) and ATP5A1 overexpression plasmids (vector or OE-ATP5A1) were sourced from Hanheng Biotechnology Co., Ltd. (Shanghai, China). The si-ATP5A1 sense strand sequence was 5'-CGGUAUCAUUCCUCGAAUUTT-3', and the antisense

 

strand sequence was 5'-AAUUCGAGGAAUGAUACCGTT-3'. The 5-μg plasmid or 3-μg siRNA and 5 μL LipoFiter3.0 were combined and incubated at room temperature for 20 minutes before being introduced to a six-well plate containing cells (200,000 to 300,000 per well). Transfection of siRNA into 769-P cells was performed using Gibco® Opti-MEM Reduced Serum Medium and LipoFiter3.0, while the overexpression plasmid was transfected into CAKI-1 and 786-O cells. The culture was then maintained at 37 ℃ with 5% $CO_2$ for 6 hours. Following a medium change, the cells were cultured for an additional 48 hours before proceeding with subsequent experiments. Transfection efficiency was evaluated via RT-PCR and WB analyses.

### *Wound-healing assay*

After transfection, 786-O, CAKI-1, and 769-P cells were seeded at a density of 500,000 cells per well in 6-well plates. Upon reaching over 90% confluence, a 200 μL pipette tip was used to swiftly create a scratch in the cell monolayer, followed by three PBS washes. The cells were then incubated in serum-free medium. Scratch wound healing was monitored under an inverted microscope, with images captured at 0, 24, and 48 hours.

### *Cell counting kit-8 (CCK-8) cell proliferation assay*

After transfection of the three cell types following the established protocol, cells were seeded into a 96-well plate at a density of 3,000–5,000 cells per well. Each well received 100 μL of medium supplemented with 10% serum and 10 μL of CCK-8 reagent, and the plate was incubated at 37 ℃ with 5% $CO_2$. Cell proliferation was assessed at 0, 24, 48, and 72 hours post-incubation, with absorbance measured at 450 nm using a microplate reader.

### *Transwell cell invasion assay*

Transfected cells were suspended in a serum-free medium to achieve a concentration of 30,000–50,000 cells/mL. A 200 μL aliquot of the cell suspension was then placed in the upper chamber of a transwell insert, while 500 μL of media supplemented with 20% FBS was added to the lower chamber. The setup was incubated for 48 hours at 37 ℃ with 5% $CO_2$. Post-incubation, cells were fixed with 4% paraformaldehyde for 15 minutes and subsequently stained with crystal violet for an additional 15 minutes. After thorough washing to remove excess reagents, images were acquired using an inverted microscope and analyzed with ImageJ software.

### *Flow cytometric analysis of cell apoptosis*

The 769-P and 786-O cells were transfected with si-RNA and plasmids, respectively, and were further cultured until the cell count reached between 1,000,000 and 3,000,000 for the experiment. On one hand, cell suspensions for both the experimental and control groups were prepared through methods such as cell dissociation, washing, and centrifugation. To the control cells, 500 μL of an Apoptosis Positive Control Solution (MultiSciences) was added, followed by incubation for 30 minutes. An equal volume of live cells was then mixed in, and the mixture was divided evenly into three tubes. These tubes were used to adjust the fluorescence channel voltage and compensation settings on the flow cytometer. On the other hand, cell suspensions were prepped in advance, ensuring that each flow cytometry tube contained 500,000 to 1,000,000 cells from either the experimental or control group. The cells were resuspended in 500 μL of Binding Buffer, followed by the addition of 5 μL of Annexin V-APC and 10 μL of 7-AAD to each tube. The tubes were incubated in the dark for 5 minutes. Finally, the apoptosis status of the cells was detected using a flow cytometer.

### *Statistical analysis*

Gene expression data analysis was conducted using R software (version 4.3.2). Image processing was performed with Image J (version 1.52a), while statistical analyses were executed using GraphPad Prism (version 9.5.1; Dotmatics). Survival curves were generated using the Kaplan-Meier method, with statistical differences assessed via the log-rank test. The "rms" package in R was utilized to develop a logistic regression prediction model and nomogram, followed by the creation of a calibration curve to evaluate the diagnostic significance of *ATP5A1* for ccRCC prognosis and to validate the model's accuracy. *ATP5A1*'s potential as an independent prognostic biomarker was evaluated through univariate and multivariate Cox survival regression analyses. Variations in mean values between two datasets were compared using Student's *t*-test. Experiments were conducted in triplicate, with results presented as mean ± standard deviation. Student's *t*-test was used to compare the differences between groups of *in vitro* experimental data. Statistical significance was determined at $P<0.05$.

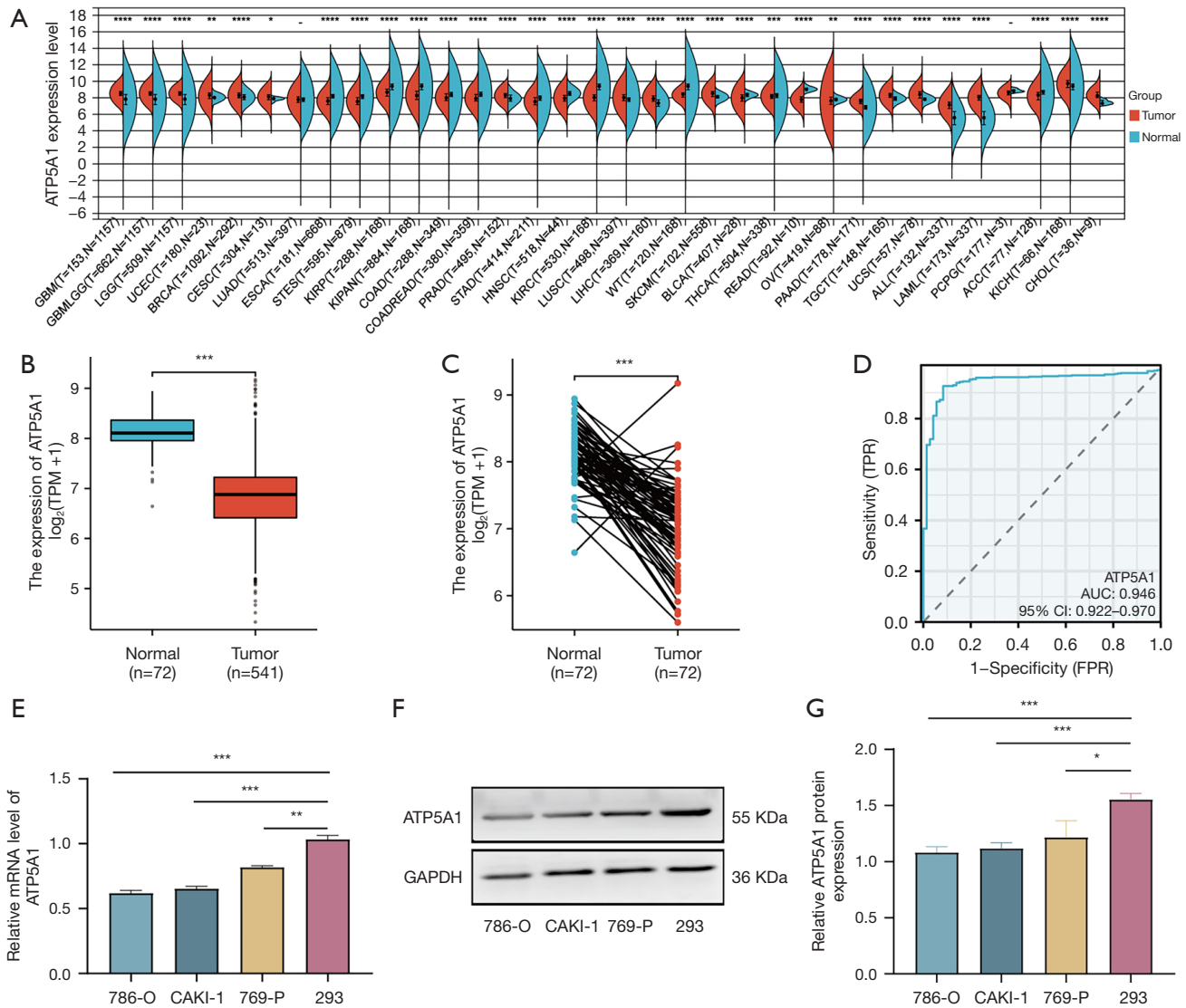


**Figure 1** Downregulation of *ATP5A1* in ccRCC. (A) The mRNA expression of *ATP5A1* across various human tumors, as derived from the TCGA database, is presented. (B,C) Unpaired and paired analyses to compare *ATP5A1* expression levels in ccRCC using TCGA data. (D) The ROC curve, reflecting the diagnostic relevance of ATP5A1 expression. (E) The mRNA expression levels of *ATP5A1* in 293 cells versus ccRCC cells are depicted. (F and G) Protein expression levels of ATP5A1 in 293 cells and ccRCC cells are displayed. *, P<0.05 *vs.* 293 cells; **, P<0.01 *vs.* 293 cells; ***, P<0.001 *vs.* 293 cells; *ATP5A1*, adenosine triphosphate synthase F1 subunit α; ccRCC, clear cell renal cell carcinoma; TCGA, The Cancer Genome Atlas; TPM, transcripts per million; ROC, receiver operating characteristic; TPR, true positive rate; FPR, false positive rate; AUC, area under the curve; CI, confidence interval.

## Results

### *ATP5A1 expression is downregulated in ccRCC*

RNA sequencing (RNAseq) data from 34 tumor projects within the TCGA dataset were downloaded and processed to obtain transcripts per million (TPM)-format data, enabling a comprehensive analysis of *ATP5A1* expression across various human cancers and normal tissues. This analysis demonstrated elevated *ATP5A1* expression in 17 cancer types, including glioma, breast invasive carcinoma, and prostate adenocarcinoma. Conversely, significant downregulation of *ATP5A1* expression was observed in 15 tumor types, such as esophageal carcinoma, colon adenocarcinoma, stomach adenocarcinoma, and

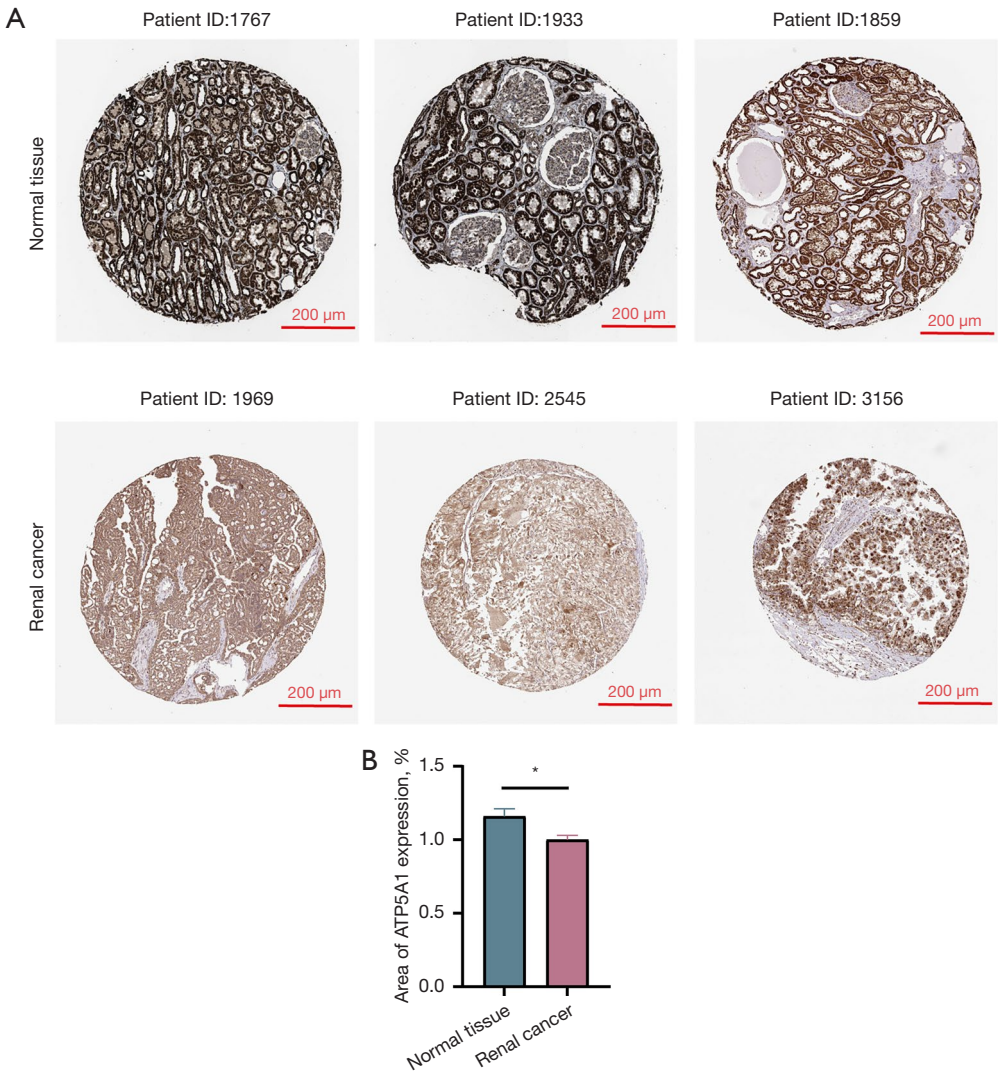


**Figure 2** Reduced ATP5A1 expression levels in ccRCC. (A) Immunohistochemical analysis data for ATP5A1 expression in normal renal tissues and ccRCC tissues were sourced from the Human Protein Atlas database (https://www.proteinatlas.org/). (B) Quantitative immunohistochemical analysis is presented; the scale bar corresponds to 200 μm. *, P<0.05 *vs.* normal tissue. Patient ID: 1767 (https://images.proteinatlas.org/13067/31200_A_8_5.jpg). Patient ID: 1933 (https://images.proteinatlas.org/13067/31200_A_9_5.jpg). Patient ID: 1859 (https://images.proteinatlas.org/44202/126704_A_7_5.jpg). Patient ID: 1969 (https://images.proteinatlas.org/40622/125073_A_9_1.jpg). Patient ID: 2545 (https://images.proteinatlas.org/40622/125073_A_7_2.jpg). Patient ID: 3156 (https://images.proteinatlas.org/40622/125073_A_9_8.jpg). ATP5A1, adenosine triphosphate synthase F1 subunit α; ccRCC, clear cell renal cell carcinoma.

ccRCC (*Figure 1A*). Additionally, RNAseq data for ccRCC were specifically retrieved and compiled from the TCGA-Kidney Renal Clear Cell Carcinoma (KIRC) dataset, focusing on TPM-format data. Initial unpaired analysis of ATP5A1 expression in cancerous versus normal tissues, and subsequent paired analysis in 72 tissue pairs of cancer and paracancerous samples, both revealed reduced ATP5A1 levels in ccRCC (*Figure 1B,1C*). Receiver operating characteristic (ROC) curve analysis demonstrated the robust diagnostic potential of *ATP5A1* for ccRCC, with an area under the curve (AUC) of 0.946 (*Figure 1D*). *In vitro* experiments utilizing 293 cells and the 786-O, CAKI-1, and 769-P renal cancer cell lines confirmed significantly lower *ATP5A1* mRNA expression (*Figure 1E*) and protein levels (*Figure 1F,1G*) in ccRCC cells compared to normal cells. Additionally, immunohistochemical data for ATP5A1 in

both ccRCC and normal kidney tissue were extracted from the HPA database, demonstrating low ATP5A1 expression in ccRCC, consistent with its messenger RNA (mRNA) expression level (*Figure 2*). Subsequent immunofluorescence assays corroborated these findings, showing that *ATP5A1* abundance in 293 cells exceeded that in the other three renal cancer cell lines (*Figure 3A-3E*).

### *Association between ATP5A1 and the clinicopathological features of ccRCC*

RNAseq data for the TCGA KIRC project were retrieved from the TCGA database and analyzed, revealing significant correlations between *ATP5A1* mRNA expression and the T stage, M stage, as well as pathological staging and grading of ccRCC. Additionally, notable differences in overall survival (OS) rates were identified (*Table 2*). Higher *ATP5A1* mRNA expression levels were associated with reductions in pathological staging severity, clinical analysis outcomes, and histological grading likelihood (*Figure 4A-4D*).

The association between *ATP5A1* expression and clinical outcomes in individuals with ccRCC was investigated to elucidate *ATP5A1*'s role in the disease's physiological behavior. Additionally, reduced *ATP5A1* expression was significantly correlated with OS [hazard ratio (HR): 0.42; 95% confidence interval (CI): 0.31–0.58], disease-specific survival (DSS) (HR: 0.22; 95% CI: 0.14–0.35), and progression-free interval (PFI) (HR: 0.36; 95% CI: 0.26–0.50) in ccRCC patients (*Figure 4E-4G*). Initially, a univariate Cox regression analysis was carried out, revealing that patients with elevated expression of *ATP5A1* exhibited improved OS (HR: 0.424; 95% CI: 0.310–0.581). Subsequently, a multivariate Cox regression analysis was conducted, confirming *ATP5A1* was an independent OS protective maker in ccRCC (HR: 0.467; 95% CI: 0.292–0.746; P=0.001) (*Table 3*). Additionally, R software (version 4.3.2) was utilized to generate a nomogram incorporating *ATP5A1* expression levels to estimate 1-, 3-, and 5-year survival probabilities in ccRCC patients (*Figure 4H*). The model demonstrated robust predictive performance, with a C-index of 0.782 (range: 0.760–0.804), and calibration plots confirmed the accuracy of the predictions (*Figure 4I*). Ultimately, low *ATP5A1* expression was significantly correlated with poor prognosis in ccRCC, highlighting its potential as a prognostic biomarker.

### *ATP5A1 suppresses migration, proliferation, invasion, and promotes apoptosis in ccRCC cells*

The role of *ATP5A1* in promoting malignant behavior in ccRCC was assessed using *in vitro* experiments with 786-O, CAKI-1, and 769-P cell lines, where *ATP5A1* was either overexpressed or knocked down. The effectiveness of *ATP5A1* modulation was confirmed through RT-PCR and WB analyses (*Figure 5A-5G*). Wound healing assays revealed a marked increase in migratory capacity in the knockdown group compared to the overexpression group (*Figure 6A-6F*). CCK-8 proliferation assays indicated that cell proliferation was significantly elevated in the knockdown group relative to the normal control (NC) group, while the overexpression group exhibited reduced proliferative capacity compared to the NC group (*Figure 7A-7C*). Additionally, transwell invasion assays showed enhanced invasive potential in cells with *ATP5A1* knockdown compared to NC group (*Figure 7D-7G*). Flow cytometry analysis revealed a decrease in apoptosis rates in ccRCC cells following *ATP5A1* knockdown, while overexpression of *ATP5A1* significantly elevated apoptosis rates (*Figure 8*).

### *ATP5A1 enrichment analysis of co-expressed genes and its association with the Wnt/β-catenin signaling pathway*

To investigate the physiological roles of the *ATP5A1* gene in ccRCC, co-expressed genes were identified using the cBioPortal database, as detailed in Table S1. A total of 105 co-expressed genes were identified, comprising 72 positively correlated and 33 negatively correlated genes. The role of *ATP5A1* in ccRCC progression was further elucidated through Gene Ontology (GO) and Kyoto Encyclopedia of Genes and Genomes (KEGG) enrichment analyses. GO enrichment analysis revealed that the majority of co-expressed genes were involved in processes such as 'mitochondrial matrix', 'mitochondrial protein processing', 'aerobic respiration', and 'lyase activity'. KEGG pathway enrichment analysis of co-expressed genes primarily identified pathways related to 'carbon metabolism', the 'citrate cycle (TCA cycle)', 'chemical carcinogenesis reactive oxygen species', and other physiological processes (*Figure 9A*). *ATP5A1* was classified based on expression levels, gene expression profiles, and phenotype, followed

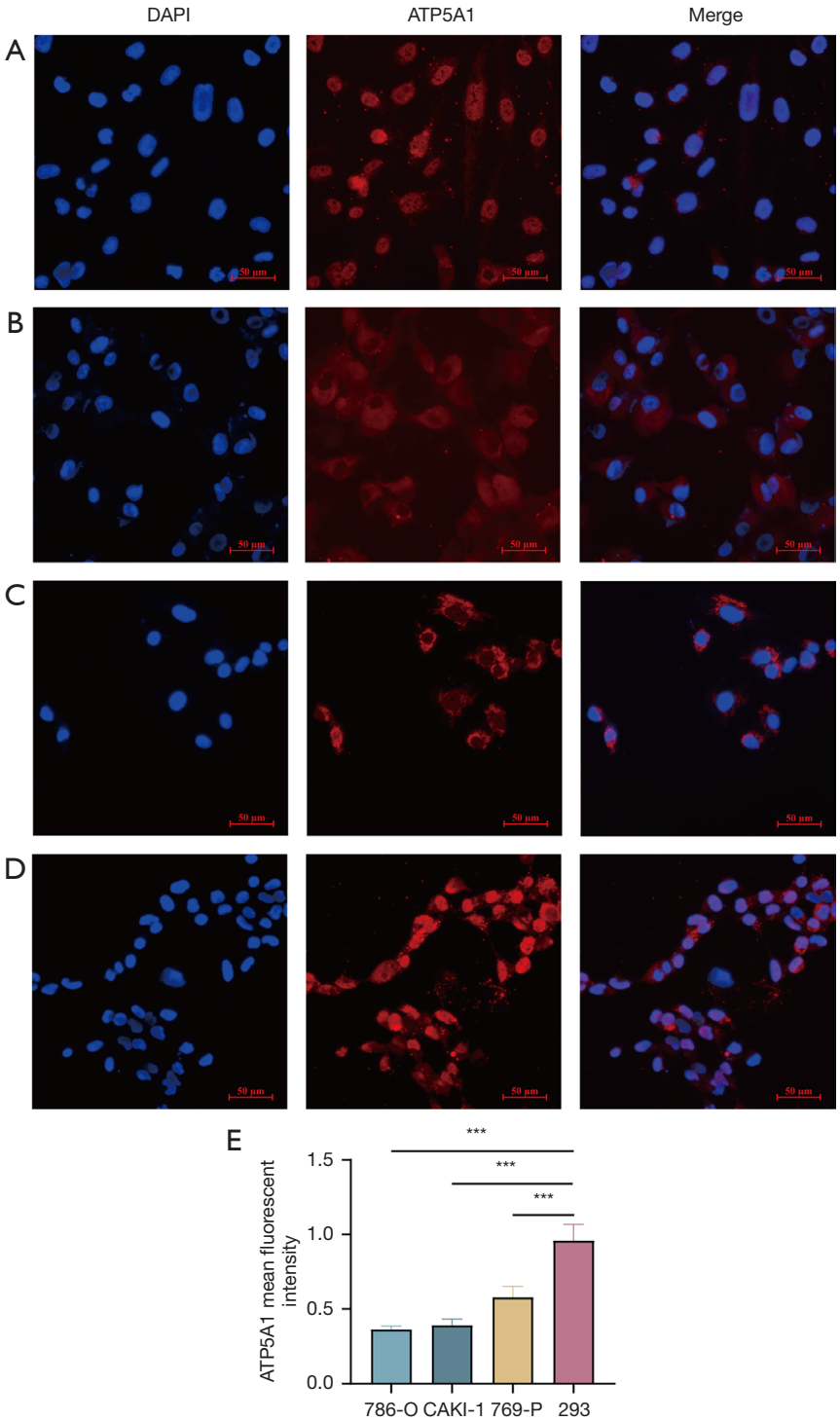


**Figure 3** Immunofluorescence analysis of ATP5A1 expression abundance in various cells. Immunofluorescence images of (A) 786-O cells, (B) CAKI-1 cells, (C) 769-P cells, and (D) 293 cells are displayed. (E) Relative quantitative analysis of mean fluorescence intensity. The scale bar corresponds to 50 μm. ***, P<0.001 *vs.* 293 cells. ATP5A1, adenosine triphosphate synthase F1 subunit α; DAPI, 4',6-diamidino-2-phenylindole.

**Table 2** Clinical characteristics of patients with ccRCC

| Characteristic | Low expression of ATP5A1 (n=270) | High expression of ATP5A1 (n=271) | P value[†] |
|---|---|---|---|
| Age (years), n (%) | | | 0.76 |
| ≤60 | 136 (25.1) | 133 (24.6) | |
| >60 | 134 (24.8) | 138 (25.5) | |
| Gender, n (%) | | | <0.001 |
| Female | 76 (14.0) | 111 (20.5) | |
| Male | 194 (35.9) | 160 (29.6) | |
| Pathologic T stage, n (%) | | | <0.001 |
| T1 | 107 (19.8) | 172 (31.8) | |
| T2 | 37 (6.8) | 34 (6.3) | |
| T3 | 119 (22.0) | 61 (11.3) | |
| T4 | 7 (1.3) | 4 (0.7) | |
| Pathologic N stage, n (%) | | | 0.29 |
| N0 | 118 (45.7) | 124 (48.1) | |
| N1 | 10 (3.9) | 6 (2.3) | |
| Pathologic M stage, n (%) | | | <0.001 |
| M0 | 201 (39.6) | 228 (44.9) | |
| M1 | 56 (11) | 23 (4.5) | |
| Pathologic stage, n (%) | | | <0.001 |
| Stage I | 104 (19.3) | 169 (31.4) | |
| Stage II | 28 (5.2) | 31 (5.8) | |
| Stage III | 78 (14.5) | 45 (8.4) | |
| Stage IV | 58 (10.8) | 25 (4.6) | |
| Histologic grade, n (%) | | | <0.001 |
| G1 | 4 (0.8) | 10 (1.9) | |
| G2 | 99 (18.6) | 137 (25.7) | |
| G3 | 110 (20.6) | 97 (18.2) | |
| G4 | 56 (10.5) | 20 (3.8) | |
| OS event, n (%) | | | <0.001 |
| Alive | 155 (28.7) | 211 (39) | |
| Dead | 115 (21.3) | 60 (11.1) | |

[†], the chi-squared test. *ATP5A1*, adenosine triphosphate synthase F1 subunit α; ccRCC, clear cell renal cell carcinoma; T, tumor; N, lymph node; M, metastasis; OS, overall survival.

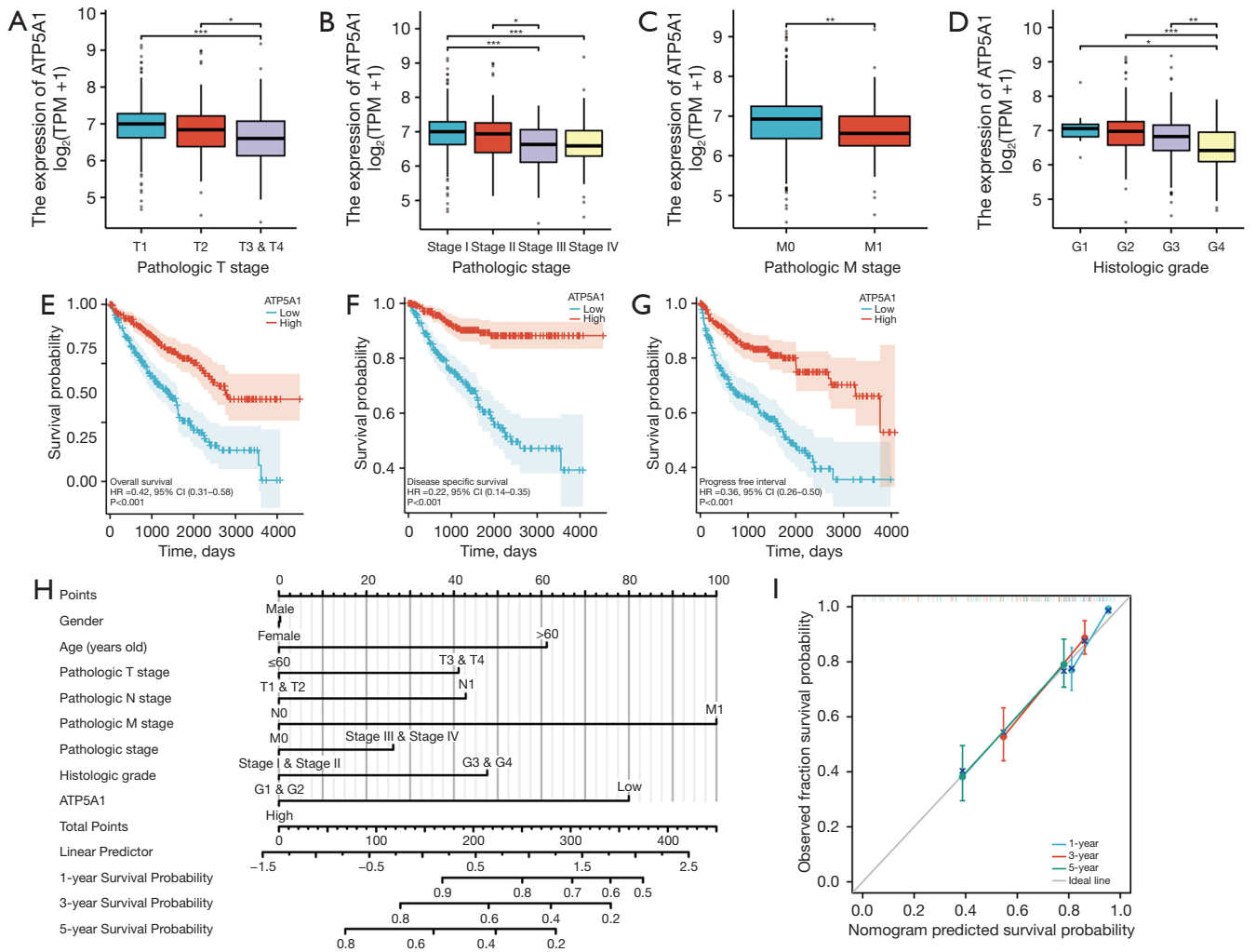


**Figure 4** Relationship between *ATP5A1* expression and the clinicopathological features of ccRCC. (A-C) The association between *ATP5A1* expression and various stages of ccRCC. (D) Association between *ATP5A1* expression and ccRCC grade stages. (E-G) The impact of *ATP5A1* expression on the survival outcomes of ccRCC patients, including OS, DSS, and PFI. Patients were stratified into high and low expression groups based on the median *ATP5A1* expression level. (H) Nomogram illustrating the association between *ATP5A1* expression and prognosis, with (I) providing a calibration plot for the nomogram regarding this association. Statistical significance is indicated as follows: *, P<0.05, T3 & T4 compared to T2, stage III compared to stage II, G4 compared to G1; **, P<0.01, M1 compared to M0, G4 compared to G3; ***, P<0.001, T3 & T4 compared to T1, stage III compared to stage I, stage V compared to stage I, G4 compared to G2. *ATP5A1*, adenosine triphosphate synthase F1 subunit α; ccRCC, clear cell renal cell carcinoma; OS, overall survival; DSS, disease-specific survival; PFI, progression-free interval; TPM, transcripts per million; T, tumor; N, lymph node; M, metastasis; CI, confidence interval; HR, hazard ratio.

by enrichment analysis using gene set enrichment analysis (GSEA) software. The results indicated significant enrichment of *ATP5A1* in signaling pathways associated with peroxisome proliferator-activated receptors (PPARs), insulin, Wnt, neurotrophin, and ErbB (*Figure 9B*).

Given the well-established link between the Wnt/β-catenin signaling pathway and the development and progression of various cancers (13,14), the mechanism by which *ATP5A1* affects ccRCC was explored. To investigate this, 769-P cells with *ATP5A1* knockdown and 786-O cells overexpressing *ATP5A1* were employed. WB analysis revealed that *ATP5A1* knockdown resulted in increased

**Table 3** Univariate and multivariate Cox regression analyses of clinical characteristics associated with overall survival

| Characteristics | Total (N) | Univariate analysis | | Multivariate analysis | |
|---|---|---|---|---|---|
| | | Hazard ratio (95% CI) | P value | Hazard ratio (95% CI) | P value |
| Age (years) | 541 | | | | |
| ≤60 | 269 | Reference | | Reference | |
| >60 | 272 | 1.791 (1.319–2.432) | <0.001 | 1.696 (1.091–2.638) | 0.02 |
| Gender | 541 | | | | |
| Female | 187 | Reference | | | |
| Male | 354 | 0.924 (0.679–1.257) | 0.61 | | |
| Pathologic T stage | 541 | | | | |
| T1 | 279 | Reference | | Reference | |
| T2 | 71 | 1.488 (0.893–2.478) | 0.13 | 0.231 (0.046–1.159) | 0.08 |
| T3 | 180 | 3.321 (2.356–4.681) | <0.001 | 0.507 (0.135–1.907) | 0.32 |
| T4 | 11 | 10.631 (5.374–21.031) | <0.001 | 0.538 (0.112–2.577) | 0.44 |
| Pathologic N stage | 258 | | | | |
| N0 | 242 | Reference | | Reference | |
| N1 | 16 | 3.422 (1.817–6.446) | <0.001 | 1.247 (0.418 - 3.720) | 0.69 |
| Pathologic M stage | 508 | | | | |
| M0 | 429 | Reference | | Reference | |
| M1 | 79 | 4.401 (3.226–6.002) | <0.001 | 0.227 (0.020–2.574) | 0.23 |
| Pathologic stage | 538 | | | | |
| Stage I | 273 | Reference | | Reference | |
| Stage II | 59 | 1.183 (0.638–2.193) | 0.59 | 3.273 (0.527–20.313) | 0.20 |
| Stage III | 123 | 2.649 (1.767–3.971) | <0.001 | 3.174 (0.779–12.925) | 0.11 |
| Stage IV | 83 | 6.622 (4.535–9.670) | <0.001 | 38.396 (2.878–512.250) | 0.006 |
| Histologic grade | 533 | | | | |
| G1 | 14 | Reference | | Reference | |
| G2 | 236 | 7,606,603.7579 (0.000–Inf) | >0.99 | 6,869,088.4698 (0.000–Inf) | >0.99 |
| G3 | 207 | 14,061,844.0831 (0.000–Inf) | >0.99 | 10,637,212.5802 (0.000–Inf) | >0.99 |
| G4 | 76 | 38,352,819.2469 (0.000–Inf) | >0.99 | 10,732,709.6651 (0.000–Inf) | >0.99 |
| ATP5A1 | 541 | | | | |
| Low | 270 | Reference | | Reference | |
| High | 271 | 0.424 (0.310–0.581) | <0.001 | 0.467 (0.292–0.746) | 0.001 |

*ATP5A1*, adenosine triphosphate synthase F1 subunit α; CI, confidence interval; T, tumor; N, lymph node; M, metastasis; OS, overall survival.

expression of β-catenin, P-GSK 3β, and c-Myc, while *ATP5A1* overexpression led to a significant decrease in the expression of these proteins (*Figure 10*).

## Discussion

The ccRCC is intimately linked to energy metabolism (15). This form of cancer is associated with the reprogramming

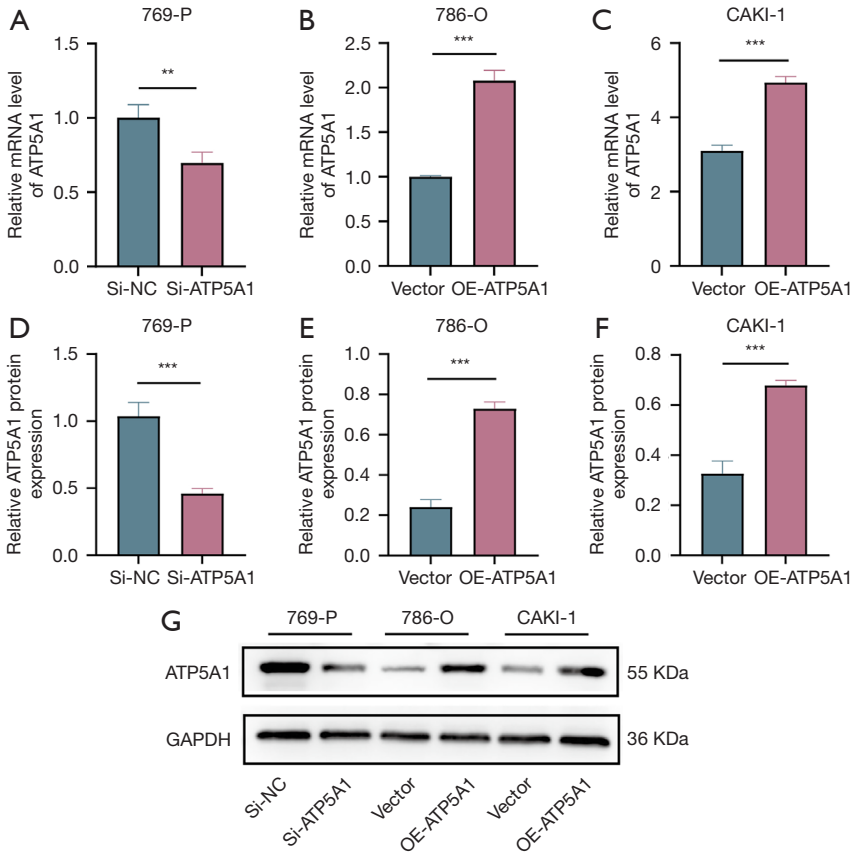


**Figure 5** Results of *ATP5A1* knockdown and overexpression. (A-C) RT-qPCR results for *ATP5A1* knockdown and overexpression in cells. (D-G) WB results under similar conditions. 'Si-NC' refers to the transfection negative control group, while 'Si-ATP5A1' denotes the Si-ATP5A1 transfected group; 'Vector' indicates the lentiviral control group; and 'OE-ATP5A1' represents the lentivirus-overexpressing *ATP5A1* group. Statistical significance is indicated as follows: **, P<0.01; ***, P<0.001 *vs.* control. *ATP5A1*, adenosine triphosphate synthase F1 subunit α; RT-qPCR, reverse transcription-quantitative polymerase chain reaction; WB, western blot.

of glucose and lipid metabolic pathways, where there is an increased allocation of metabolic flux via glycolysis within the tumor cells (16,17). Additionally, it encompasses dysfunctions in mitochondrial bioenergetics and lipid metabolism (18-20). The upregulation of glycolytic enzymes in ccRCC is a key factor that drives cancer cell proliferation and adversely affects patient survival rates (21). ATP5F1A, also known as *ATP5A1*, functions as a key component of mitochondrial ATP synthase. This enzyme complex consists of two primary domains: F [1], which contains the extracellular catalytic core, and F [0], housing the membrane proton channel. These domains are linked by central and peripheral stalks, facilitating the coupling of ATP synthesis in the F [1] domain with proton transport, driven by the rotational mechanism of the central stalk subunit (22). Unlike normal cells, malignant tumors exhibit distinct bioenergetic profiles, characterized by reduced expression of mitochondrial ATP synthase and elevated levels of glycolytic enzymes (23). Throughout the progression of human malignant tumors, oxidative phosphorylation becomes increasingly pronounced, accompanied by elevated *ATP5A1* levels. This upregulation disrupts the expression of ATP synthase subunits, subsequently diminishing mitochondrial electron chain activity and oxidative phosphorylation efficiency (9,10). In certain prostate cancers, *ATP5A1* expression is reduced, leading to the suppression of oxidative phosphorylation processes (24). Conversely, in cervical cancer, *ATP5A1* overexpression has been implicated in the disruption of alternative splicing for multiple genes involved in critical physiological processes, such as glucose homeostasis and hypoxia-inducible factor 1 signaling, thereby contributing to abnormal cancer-

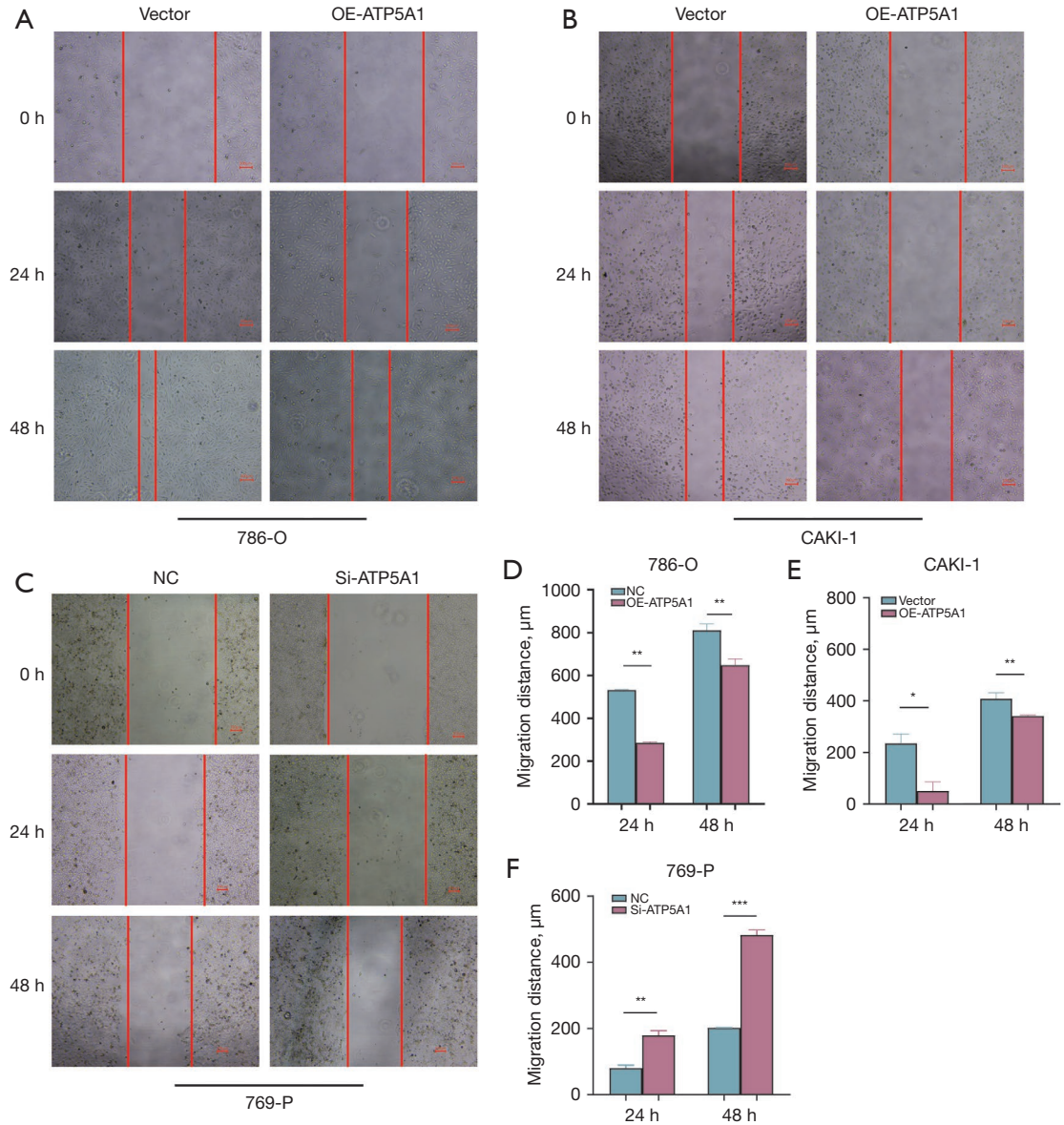


**Figure 6** *ATP5A1* inhibits ccRCC cell migration. (A-F) Wound healing assays were conducted to assess changes in migratory capacity following *ATP5A1* knockdown and overexpression (×40). The scale bar represents 100 μm. 'NC' indicates the transfection negative control group; 'Si-ATP5A1' refers to the Si-ATP5A1 transfected group; 'Vector' denotes the lentiviral control group; and 'OE-ATP5A1' represents the lentivirus-overexpressing *ATP5A1* group. *, P<0.05; **, P<0.01; ***, P<0.001 *vs.* control. *ATP5A1*, adenosine triphosphate synthase F1 subunit α; ccRCC, clear cell renal cell carcinoma.

specific RNA splicing (25). In lung adenocarcinoma patients, *ATP5A1* expression was significantly elevated in metastatic lesions compared to primary tumors, indicating its involvement in tumor progression and metastasis (26). Furthermore, analysis of mRNA expression profiles revealed that *ATP5A1* levels, along with microvascular proliferation, were notably higher in glioblastoma tumor cells compared to normal cerebrovascular cells (7).

Given the increasing complexity of tumors and the need for more precise prognostic monitoring, the tumor node metastasis (TNM) classification alone is insufficient to address the clinical demands of cancer patients (27).

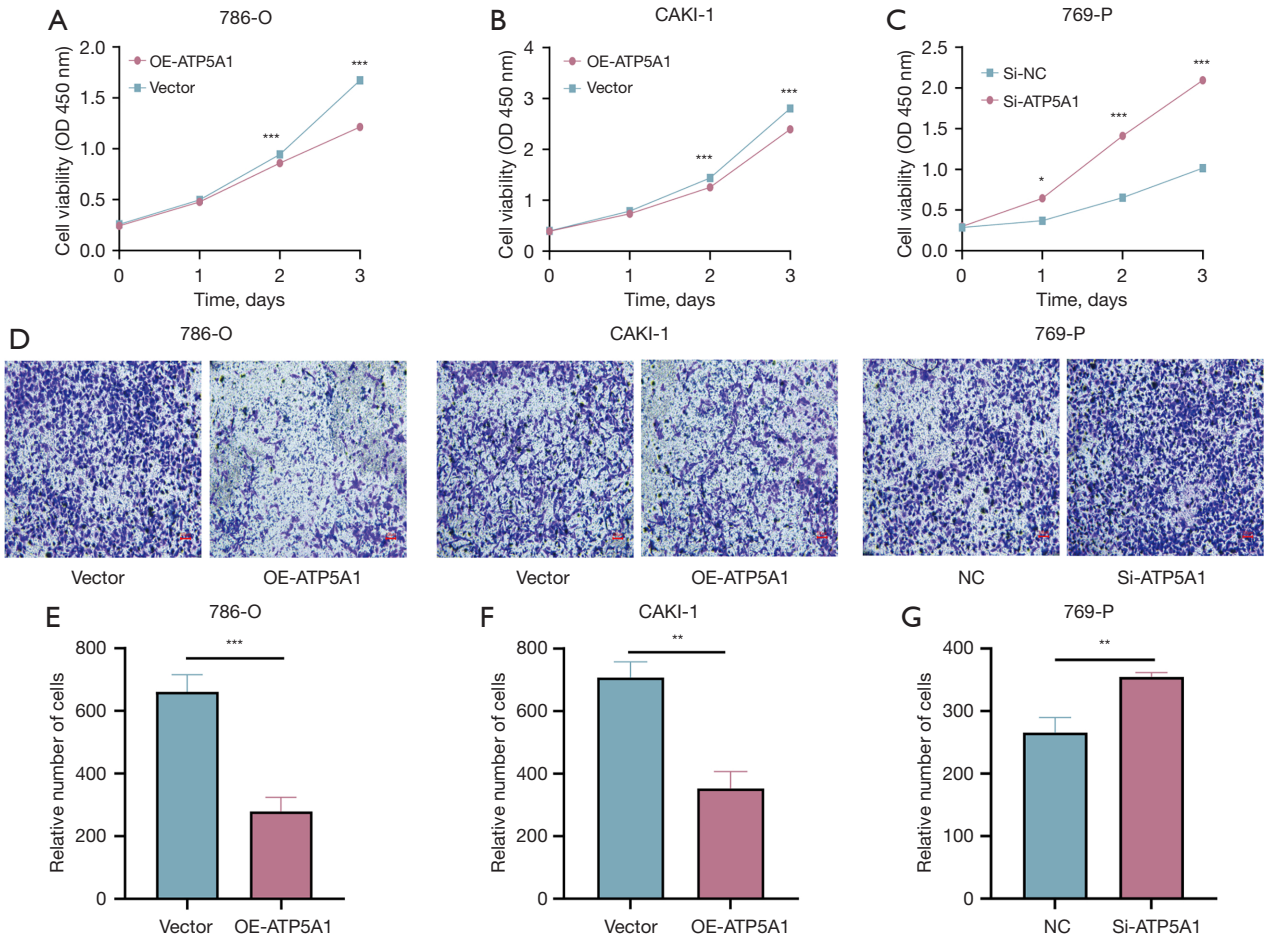


**Figure 7** Inhibitory effects of *ATP5A1* on ccRCC proliferation and invasion. (A-C) The CCK-8 assay was utilized to assess changes in cellular proliferation following *ATP5A1* knockdown and overexpression. (D-G) Transwell assays were conducted to evaluate alterations in invasive capabilities under similar conditions. The scale bar indicates 100 μm, crystal violet staining (0.1%). 'Si-NC' denotes the transfection negative control group; 'Si-ATP5A1' refers to the Si-ATP5A1 transfected group; 'Vector' represents the lentiviral control group; and 'OE-ATP5A1' corresponds to the lentivirus-overexpressing ATP5A1 group. Staining method: crystal violet. Statistical significance is indicated as follows: *, P<0.05, **, P<0.01, and ***, P<0.001, compared to control. *ATP5A1*, adenosine triphosphate synthase F1 subunit α; ccRCC, clear cell renal cell carcinoma; OD, optical density.

Consequently, contemporary clinical guidelines have incorporated various novel biomarkers to enhance the diagnosis and treatment of cancers, including prostate, gastric, and breast cancers (28-32). In contrast, ccRCC presents unique therapeutic challenges, with a notable absence of effective biomarkers for diagnosis, treatment, and prognosis due to the variability in personalized therapies and patient-specific treatment regimens (33). This highlights the ongoing necessity to identify new molecular markers for ccRCC.

The pan-cancer analysis conducted in this study identified a significant reduction in *ATP5A1* expression in various tumors, including ccRCC. Furthermore, *ATP5A1* expression demonstrated an inverse correlation with clinical stage, pathological stage, and histological grade in ccRCC, while positively correlating with prognosis. These results suggest that *ATP5A1* may act as a tumor suppressor in ccRCC. To confirm *ATP5A1* expression in ccRCC, a series of *in vitro* experiments were conducted using 293 cells and selected ccRCC cell lines, with findings consistent with those from online databases. Additionally, *ATP5A1* was found to be closely linked with pathological staging, clinical

 

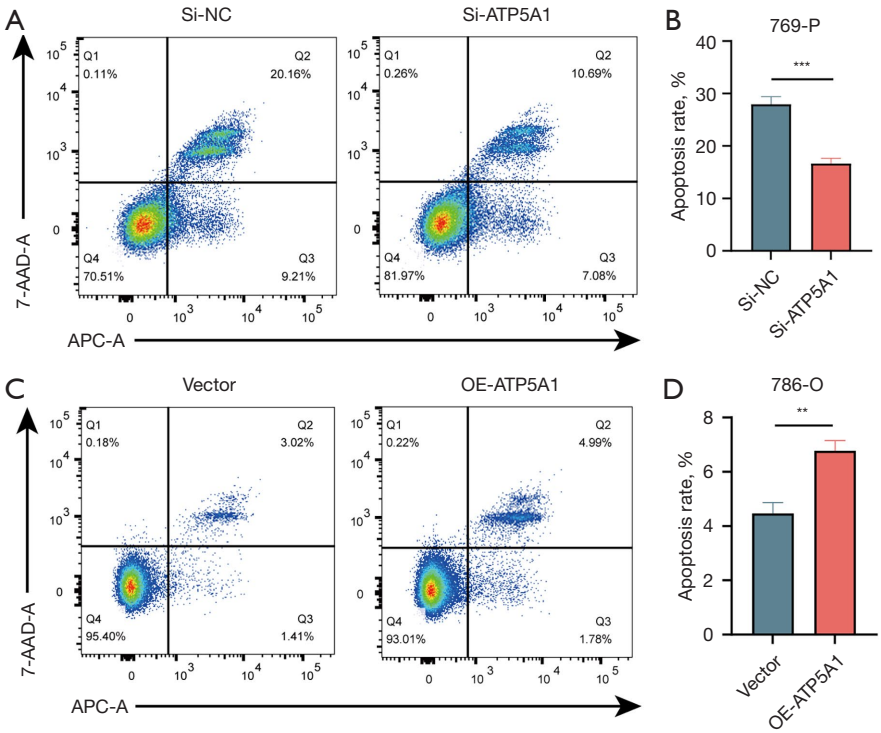


**Figure 8** Flow cytometric analysis of cell apoptosis. (A,B) The apoptosis rate of 769-P cells. (C,D) The apoptosis rate of 786-O cells. ***, P<0.001 *vs.* Si-NC group; **, P<0.01 *vs.* Vector group. 'Si-NC' denotes the transfection negative control group; 'Si-ATP5A1' refers to the Si-ATP5A1 transfected group; 'Vector' represents the lentiviral control group; and 'OE-ATP5A1' corresponds to the lentivirus-overexpressing ATP5A1 group. *ATP5A1*, adenosine triphosphate synthase F1 subunit α; APC-A, annexin V-APC fluorescence intensity; AAD-A, aminoactinomycin D fluorescence intensity.

staging, and histological grading, and may serve as an independent prognostic factor for OS in ccRCC patients. In summary, *ATP5A1* holds potential as a prognostic marker for ccRCC.

The Wnt signaling pathway plays a central role in various physiological and pathological processes, particularly in embryonic development and cell differentiation (34). Dysregulation of the Wnt/β-catenin pathway is a common factor in a wide range of diseases, including both malignant and benign conditions (35). It has been extensively linked to breast cancer proliferation and metastasis (36), various stages of glioblastoma (37), the progression of colon cancer (38), as well as ovarian, endometrial, and cervical cancers (39). Additionally, it is a key driver in the onset and progression of prostate cancer (40). In ccRCC, mutations in adenomatous polyposis coli (APC) and Axin significantly influence Wnt signaling, with VHL identified as a β-catenin target, underscoring the pathway's central role in renal cancer development (11). GO and KEGG analyses indicated that *ATP5A1* is predominantly involved in aerobic respiration and carbon metabolism. GSEA further identified a strong association between *ATP5A1* and the Wnt signaling pathway. These results suggest that *ATP5A1* may influence intracellular signal transduction and transmission, affecting tumor cell signaling and ccRCC progression via the Wnt pathway, a conclusion corroborated by Yuan *et al.* (10). WB analysis demonstrated a reduction in p-GSK-3β, a key protein in the Wnt/β-catenin pathway, along with the downstream regulatory protein c-Myc, following *ATP5A1* overexpression in ccRCC. *ATP5A1* knockdown resulted in elevated expression levels of p-GSK3β and c-Myc, suggesting that *ATP5A1* may reduce p-GSK3β and c-Myc protein levels by diminishing β-catenin activity, thus inhibiting the Wnt/β-catenin signaling pathway. Functional cytological studies further demonstrated that *ATP5A1* suppresses cell migration, proliferation, and invasion while promoting apoptosis in ccRCC cells. Collectively, this study suggests that *ATP5A1* may inhibit the Wnt/β-catenin signaling pathway, thereby impeding the malignant biological behavior of ccRCC.

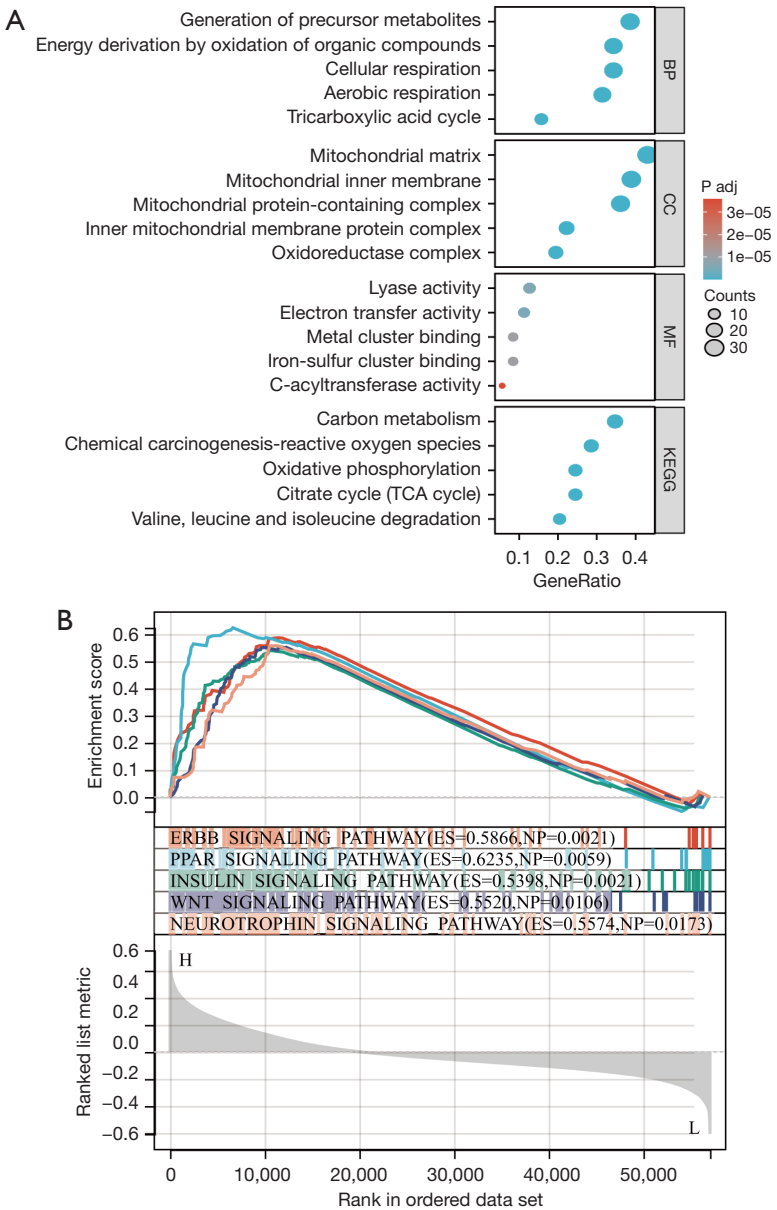


**Figure 9** Enrichment analysis of *ATP5A1* co-expressed genes. (A) A bubble plot illustrating GO and KEGG-based enrichment analysis of *ATP5A1* co-expressed genes in ccRCC. (B) GSEA enrichment analysis of *ATP5A1* co-expressed genes. KEGG, Kyoto Encyclopedia of Genes and Genomes; GSEA, gene set enrichment analysis; *ATP5A1*, adenosine triphosphate synthase F1 subunit α; ccRCC, clear cell renal cell carcinoma; BP, biological process; CC, cellular component; MF, molecular function; GO, Gene Ontology; TCA, tricarboxylic acid cycle.

Nonetheless, there are several limitations in this study. The survival rates and prognostic significance of *ATP5A1*, as derived from TCGA dataset analysis, necessitate further validation with additional clinical data to ensure robust confirmation in future research. Moreover, elucidating the precise molecular mechanisms by which *ATP5A1* influences ccRCC remains essential, highlighting the need for further detailed mechanistic studies.

## Conclusions

In summary, this study demonstrates that *ATP5A1* expression is significantly downregulated in ccRCC, exerting a suppressive influence on the malignant behavior

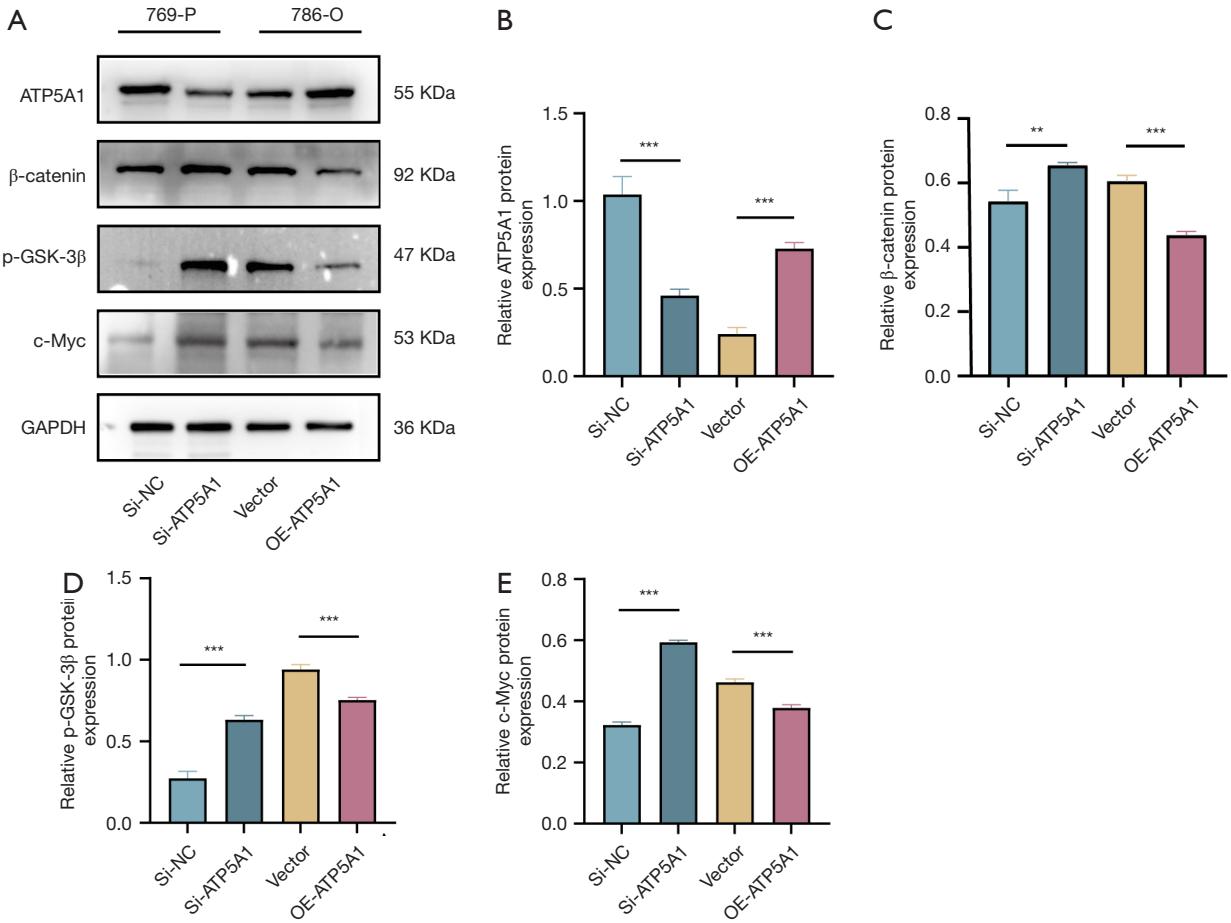


**Figure 10** *ATP5A1* correlates with the Wnt/β-catenin signaling pathway. (A) WB analysis was used to evaluate the impact of *ATP5A1* knockdown and overexpression on β-catenin, p-GSK-3β and c-Myc. The relative protein expression levels of (B) ATP5A1, (C) β-catenin, (D) p-GSK-3β protein, and (E) c-Myc were quantified. 'Si-NC' denotes the transfection negative control group; 'Si-ATP5A1' represents the Si-ATP5A1 transfected group; 'Vector' serves as the lentiviral control group; and 'OE-ATP5A1' indicates the lentivirus-overexpressing ATP5A1 group. **, P<0.01; ***, P<0.001 *vs.* control. *ATP5A1*, adenosine triphosphate synthase F1 subunit α; p-GSK-3β, phosphorylated GSK3β; WB, western blot.

of cancer cells. This downregulation indicates that *ATP5A1* expression could serve as a valuable prognostic marker. Moreover, *ATP5A1* may impede ccRCC progression by inhibiting the Wnt/β-catenin signaling pathway.

## Acknowledgments

None.

## Footnote

*Reporting Checklist:* The authors have completed the TRIPOD reporting checklist. Available at https://tcr.amegroups.com/article/view/10.21037/tcr-24-1397/rc

*Data Sharing Statement:* Available at https://tcr.amegroups.com/article/view/10.21037/tcr-24-1397/dss

*Peer Review File:* Available at https://tcr.amegroups.com/article/view/10.21037/tcr-24-1397/prf

*Funding:* None.

*Conflicts of Interest:* All authors have completed the ICMJE uniform disclosure form (available at https://tcr.amegroups.com/article/view/10.21037/tcr-24-1397/coif). The authors

have no conflicts of interest to declare.

*Ethical Statement:* The authors are accountable for all aspects of the work in ensuring that questions related to the accuracy or integrity of any part of the work are appropriately investigated and resolved. The study was conducted in accordance with the Declaration of Helsinki (as revised in 2013).



## References

1. Escudier B, Porta C, Schmidinger M, et al. Electronic address: clinicalguidelines@esmo.org. Renal cell carcinoma: ESMO Clinical Practice Guidelines for diagnosis, treatment and follow-up†. Ann Oncol 2019;30:706-20.
2. Wang Y, Suarez ER, Kastrunes G, et al. Evolution of cell therapy for renal cell carcinoma. Mol Cancer 2024;23:8.
3. Golijanin B, Malshy K, Khaleel S, et al. Evolution of the HIF targeted therapy in clear cell renal cell carcinoma. Cancer Treat Rev 2023;121:102645.
4. Wang X, Lopez R, Luchtel RA, et al. Immune evasion in renal cell carcinoma: biology, clinical translation, future directions. Kidney Int 2021;99:75-85.
5. Boyer PD. The ATP synthase--a splendid molecular machine. Annu Rev Biochem 1997;66:717-49.
6. Al-Salem AM, Saquib Q, Siddiqui MA, et al. Organophosphorus flame retardant (tricresyl phosphate) trigger apoptosis in HepG2 cells: Transcriptomic evidence on activation of human cancer pathways. Chemosphere 2019;237:124519.
7. Majercikova Z, Dibdiakova K, Gala M, et al. Different Approaches for the Profiling of Cancer Pathway-Related Genes in Glioblastoma Cells. Int J Mol Sci 2022;23:10883.
8. Kim JS, Lee D, Kim D, et al. Toxoplasma gondii GRA8-derived peptide immunotherapy improves tumor targeting of colorectal cancer. Oncotarget 2020;11:62-73.
9. Brüggemann M, Gromes A, Poss M, et al. Systematic Analysis of the Expression of the Mitochondrial ATP Synthase (Complex V) Subunits in Clear Cell Renal Cell Carcinoma. Transl Oncol 2017;10:661-8.
10. Yuan L, Chen L, Qian K, et al. A novel correlation between ATP5A1 gene expression and progression of human clear cell renal cell carcinoma identified by co-expression analysis. Oncol Rep 2018;39:525-36.
11. Chen C, Tian A, Zhao M, et al. Adenoviral delivery of VHL suppresses bone sarcoma cell growth through inhibition of Wnt/β-catenin signaling. Cancer Gene Ther 2019;26:83-93.
12. Mazzei M, Vascellari M, Zanardello C, et al. Quantitative real time polymerase chain reaction (qRT-PCR) and RNAscope in situ hybridization (RNA-ISH) as effective tools to diagnose feline herpesvirus-1-associated dermatitis. Vet Dermatol 2019;30:491-e147.
13. Piotrowska Ż, Niezgoda M, Młynarczyk G, et al. Comparative Assessment of the WNT/β-Catenin Pathway, CacyBP/SIP, and the Immunoproteasome Subunit LMP7 in Various Histological Types of Renal Cell Carcinoma. Front Oncol 2020;10:566637.
14. Parsons MJ, Tammela T, Dow LE. WNT as a Driver and Dependency in Cancer. Cancer Discov 2021;11:2413-29.
15. Lucarelli G, Loizzo D, Franzin R, et al. Metabolomic insights into pathophysiological mechanisms and biomarker discovery in clear cell renal cell carcinoma. Expert Rev Mol Diagn 2019;19:397-407.
16. De Marco S, Torsello B, Minutiello E, et al. The cross-talk between Abl2 tyrosine kinase and TGFβ1 signalling modulates the invasion of clear cell Renal Cell Carcinoma cells. FEBS Lett 2023;597:1098-113.
17. Lucarelli G, Rutigliano M, Loizzo D, et al. MUC1 Tissue Expression and Its Soluble Form CA15-3 Identify a Clear Cell Renal Cell Carcinoma with Distinct Metabolic Profile and Poor Clinical Outcome. Int J Mol Sci 2022;23:13968.
18. di Meo NA, Lasorsa F, Rutigliano M, et al. The dark side of lipid metabolism in prostate and renal carcinoma: novel insights into molecular diagnostic and biomarker discovery. Expert Rev Mol Diagn 2023;23:297-313.
19. Bianchi C, Meregalli C, Bombelli S, et al. The glucose and lipid metabolism reprogramming is grade-dependent in clear cell renal cell carcinoma primary cultures and is targetable to modulate cell viability and proliferation. Oncotarget 2017;8:113502-15.
20. Bombelli S, Torsello B, De Marco S, et al. 36-kDa Annexin A3 Isoform Negatively Modulates Lipid Storage in Clear Cell Renal Cell Carcinoma Cells. Am J Pathol 2020;190:2317-26.

21. Lucarelli G, Rutigliano M, Sallustio F, et al. Integrated multi-omics characterization reveals a distinctive metabolic signature and the role of NDUFA4L2 in promoting angiogenesis, chemoresistance, and mitochondrial dysfunction in clear cell renal cell carcinoma. Aging (Albany NY) 2018;10:3957-85.
22. Xue J, Li Y, Qi Y, et al. Exogenous Otx2 protects midbrain dopaminergic neurons from MPP(+) by interacting with ATP5a1 and promoting ATP synthesis. Neurotoxicology 2022;91:211-7.
23. Huang M, Yang L, Peng X, et al. Autonomous glucose metabolic reprogramming of tumour cells under hypoxia: opportunities for targeted therapy. J Exp Clin Cancer Res 2020;39:185.
24. Fu J, Liu G, Zhang X, et al. TRPM8 promotes hepatocellular carcinoma progression by inducing SNORA55 mediated nuclear-mitochondrial communication. Cancer Gene Ther 2023;30:738-51.
25. Song Ba Y, Wang Ma F, Wei Ma Y, et al. ATP5A1 Participates in Transcriptional and Posttranscriptional Regulation of Cancer-Associated Genes by Modulating Their Expression and Alternative Splicing Profiles in HeLa Cells. Technol Cancer Res Treat 2021;20:15330338211039126.
26. Pasternack H, Polzer M, Gemoll T, et al. Proteomic analyses identify HK1 and ATP5A to be overexpressed in distant metastases of lung adenocarcinomas compared to matched primary tumors. Sci Rep 2023;13:20948.
27. Aho J, Reisenauer J. Additional Patient Factors may Predict Survival in Esophageal Cancer Better than TMN Alone After Esophagectomy. Ann Surg Oncol 2019;26:3423-4.
28. Sarhadi VK, Armengol G. Molecular Biomarkers in Cancer. Biomolecules 2022;12:1021.
29. Boehm BE, York ME, Petrovics G, et al. Biomarkers of Aggressive Prostate Cancer at Diagnosis. Int J Mol Sci 2023;24:2185.
30. Nevo A, Navaratnam A, Andrews P. Prostate cancer and the role of biomarkers. Abdom Radiol (NY) 2020;45:2120-32.
31. Neves Rebello Alves L, Dummer Meira D, Poppe Merigueti L, et al. Biomarkers in Breast Cancer: An Old Story with a New End. Genes (Basel) 2023;14:1364.
32. de Mello RA, Amaral GA, Neves NM, et al. Current and potential biomarkers in gastric cancer: a critical review of the literature. Future Oncol 2021;17:3383-96.
33. Deleuze A, Saout J, Dugay F, et al. Immunotherapy in Renal Cell Carcinoma: The Future Is Now. Int J Mol Sci 2020;21:2532.
34. Hayat R, Manzoor M, Hussain A. Wnt signaling pathway: A comprehensive review. Cell Biol Int 2022;46:863-77.
35. Liu J, Xiao Q, Xiao J, et al. Wnt/β-catenin signalling: function, biological mechanisms, and therapeutic opportunities. Signal Transduct Target Ther 2022;7:3.
36. Xu X, Zhang M, Xu F, et al. Wnt signaling in breast cancer: biological mechanisms, challenges and opportunities. Mol Cancer 2020;19:165.
37. Latour M, Her NG, Kesari S, et al. WNT Signaling as a Therapeutic Target for Glioblastoma. Int J Mol Sci 2021;22:8428.
38. Zhao H, Ming T, Tang S, et al. Wnt signaling in colorectal cancer: pathogenic role and therapeutic target. Mol Cancer 2022;21:144.
39. McMellen A, Woodruff ER, Corr BR, et al. Wnt Signaling in Gynecologic Malignancies. Int J Mol Sci 2020;21:4272.
40. Koushyar S, Meniel VS, Phesse TJ, et al. Exploring the Wnt Pathway as a Therapeutic Target for Prostate Cancer. Biomolecules 2022;12:309.

**Cite this article as:** Zhou W, Tang Q, Wu J, Huang M, Huang Q, Qin T, Tang N, Gai S. *ATP5A1* as a potential prognostic biomarker in clear-cell renal cell carcinoma. Transl Cancer Res 2025;14(2):1246-1264. doi: 10.21037/tcr-24-1397